Chapter 9

Optical fibers and optical amplifiers

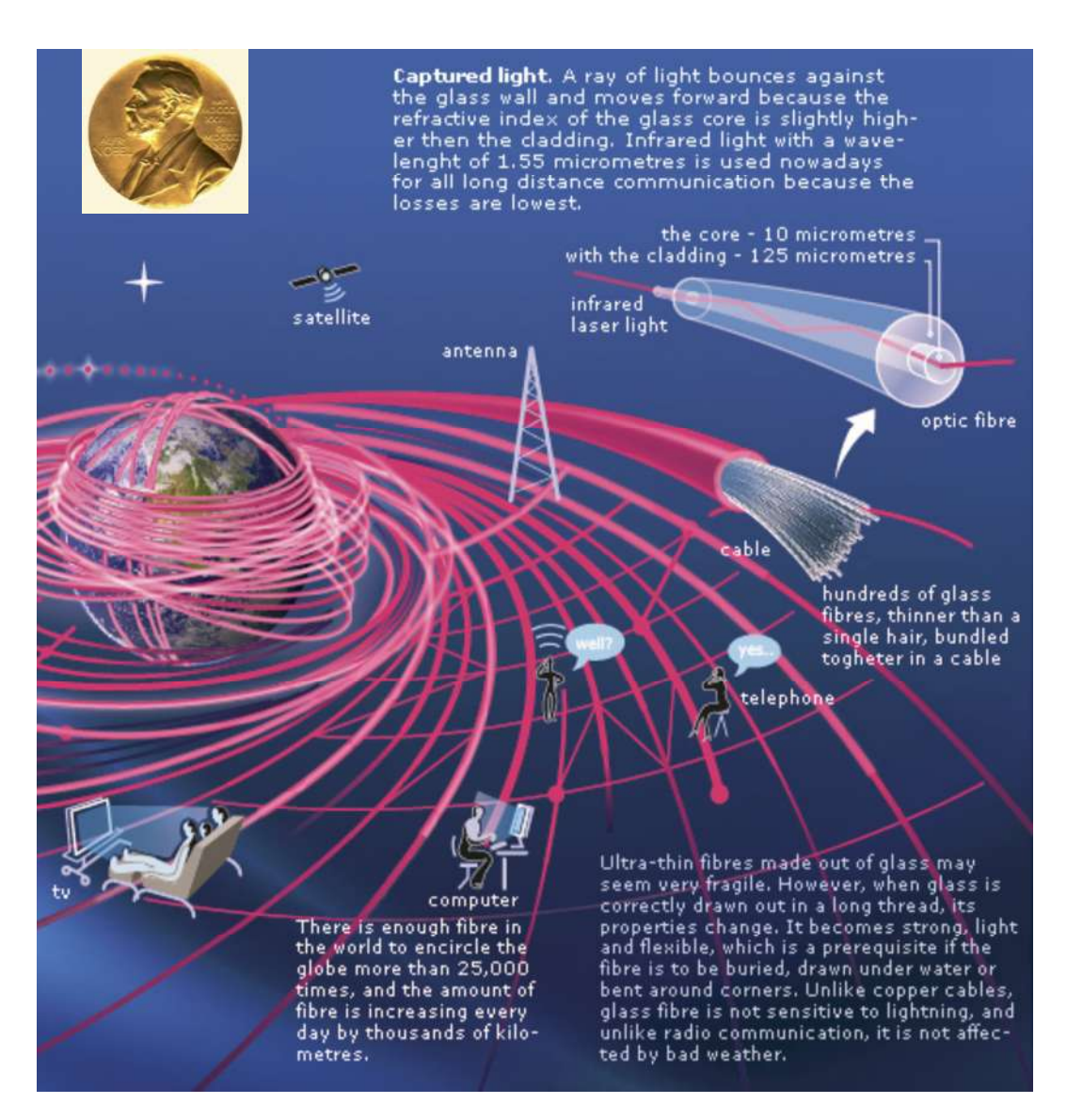


Figure 9.1: Nobel prize in physics 2009 for "for groundbreaking achievements concerning the transmission of light in fibers for optical communication" to Charles Kuen Kao

9.1 Historical perspective and fiber optical fabrication¹

Historical Perspective

Total internal reflection - the basic phenomenon responsible for guiding of light in optical fibers - is known from the nineteenth century. The reader is referred to a 1999 book for the interesting history behind the discovery of this phenomenon. Although uncladded glass fibers were fabricated in the 1920s, the field of fiber optics was not born until the 1950s when the use of a cladding layer led to considerable improvement in the fiber characteristics. The idea that optical fibers would benefit from a dielectric cladding was not obvious and has a remarkable history.

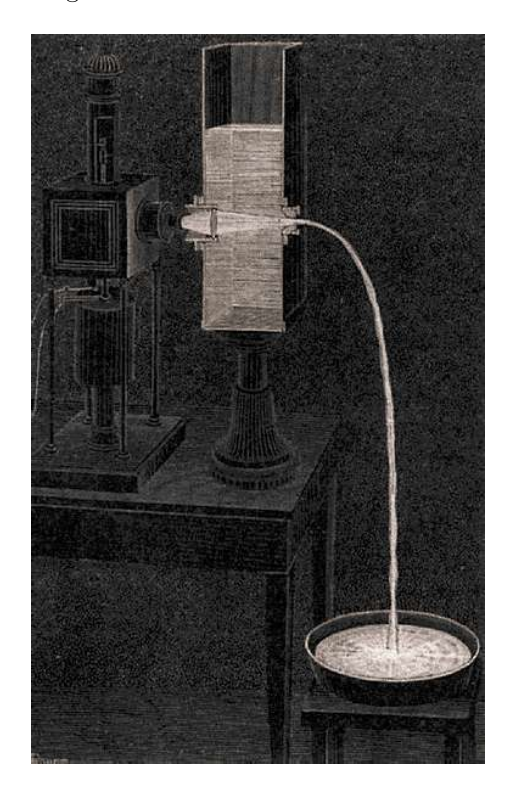


Figure 9.2: Daniel Colladon first described this "light fountain" or "light pipe" in an 1842 article entitled On the reflections of a ray of light inside a parabolic liquid stream. This particular illustration comes from a later article by Colladon, in 1884.²

The field of fiber optics developed rapidly during the 1960s, mainly for the purpose of image transmission through a bundle of glass fibers . These early fibers were extremely lossy (loss >1000 dB/km) from the modern standard. However, the situation changed drastically in 1970 when, following an earlier suggestion, losses of silica fibers were reduced to below 20 dB/km . Further progress in fabrication technology resulted by 1979 in a loss of only 0.2 dB/km in the 1.55 μ m wavelength region, a loss level limited mainly by the fundamental process of Rayleigh scattering.

The availability of low-loss silica fibers led not only to a revolution in the field of optical fiber communications but also to the advent of the new field of nonlinear fiber optics. Stimulated Raman- and Brillouin-scattering processes in optical fibers were studied as early as 1972. This work stimulated the study of other nonlinear phenomena such as optically induced birefringence, parametric four-wave mixing, and self-phase modulation. An important contribution was made in 1973 when it was suggested that optical fibers can support soliton-like pulses as a result of an interplay between the dispersive and nonlinear effects. Optical solitons were observed in a 1980 experiment and led to a number of advances during the 1980s in the generation and control of ultrashort optical pulses. The decade of the 1980s also saw the development of pulse-compression and optical-switching techniques that exploited the nonlinear effects in fibers. Pulses as short as

 $^{^1{\}rm Chapter~1~(Page~1-13)}$ - Nonlinear fiber optics - Agrawal, G. P. Govind P. - Oxford : Academic Press, 2012 $^2{\rm Source:~http://en.wikipedia.org/wiki/Optical_fiber}$

6 fs were generated by 1987. Several reviews and books cover the enormous progress made during the 1980s.

The field of nonlinear fiber optics continued to grow during the decade of the 1990s. A new dimension was added when optical fibers were doped with rare-earth elements and used to make amplifiers and lasers. Although fiber amplifiers were made as early as 1964, it was only after 1987 that their development accelerated. Erbium-doped fiber amplifiers attracted the most attention because they operate in the wavelength region near 1.55 μ m and can be used for compensation of losses in fiber-optic lightwave systems. Such amplifiers were used for commercial applications beginning in 1995. Their use has led to a virtual revolution in the design of multichannel lightwave systems.

The advent of fiber amplifiers also fueled research on optical solitons and led eventually to the concept of dispersion-managed solitons. In another development, fiber gratings, first made in 1978, were developed during the 1990s to the point that they became an integral part of lightwave technology. Nonlinear effects in fiber gratings and photonic-crystal fibers have attracted considerable attention since 1996. Clearly, the field of nonlinear fiber optics has grown considerably in the 1990s and is expected to do so during the twenty-first century. It has led to a number of advances important from the fundamental as well as the technological point of view. The interest in nonlinear fiber optics should continue in view of the development of the photonic-based technologies for information management.

Fiber Characteristics

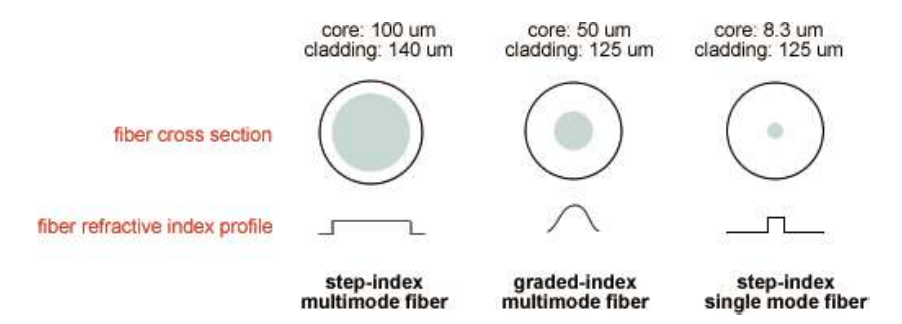


Figure 9.3: Cross section and the refractive-index profile of a step-index, graded index and step index single mode fiber.

In its simplest form, an optical fiber consists of a central glass core surrounded by a cladding layer whose refractive index n_2 is slightly lower than the core index n_1 . Such fibers are generally referred to as step-index fibers to distinguish them from graded-index fibers in which the refractive index of the core decreases gradually from center to core boundary. Figure 1.1 shows schematically the cross section and refractive-index profile of a step-index fiber. Two parameters that characterize an optical fiber are the relative core-cladding index difference

$$\Delta = \frac{n_1 - n_2}{n_1} \tag{9.1.1}$$

and the so-called V parameter defined as

$$V = k_0 a (n_1^2 - n_2^2)^{1/2} (9.1.2)$$

where $k_0 = 2\pi/\lambda$, a is the core radius, and λ is the wavelength of light.

The V parameter determines the number of modes supported by the fiber. Step-index fiber supports a single mode if V < 2.405. Optical fibers designed to satisfy this condition are called single-mode fibers. The main difference between the single-mode and multimode fibers is the core size. The core radius a is typically 2530 μ m for multimode fibers. However, single-mode fibers with $\Delta \approx 0.003$ require a to be $< 5\mu$ m. The numerical value of the outer radius b is less critical as long as it is large enough to confine the fiber modes entirely. A standard value of $b = 62.5\mu$ m is commonly used for both single-mode and multimode fibers. Since nonlinear effects are mostly

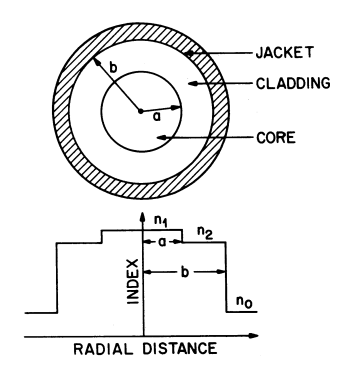


Figure 9.4: Schematic illustration of the cross section and the refractive-index profile of a stepindex fiber.

studied using single-mode fibers, the term optical fiber in this text refers to single-mode fibers unless noted otherwise.

Material and Fabrication



Figure 9.5: Cabled Fibers used in industry

The material of choice for low-loss optical fibers is pure silica glass synthesized by fusing SiO_2 molecules. The refractive-index difference between the core and the cladding is realized by the selective use of dopants during the fabrication process. Dopants such as GeO_2 and P_2O_5 increase the refractive index of pure silica and are suitable for the core, while materials such as boron and fluorine are used for the cladding because they decrease the refractive index of silica. Additional dopants can be used depending on specific applications. For example, to make fiber amplifiers and lasers, the core of silica fibers is codoped with rare-earth ions using dopants such as $ErCl_3$ and Nd_2O_3 . Similarly, Al_2O_3 is sometimes added to control the gain spectrum of fiber amplifiers.

The fabrication of optical fibers involves two stages. In the first stage, a vapor-deposition method is used to make a cylindrical preform with the desired refractive-index profile and the relative core-cladding dimensions. A typical preform is 1-m long with 2-cm diameter. In the second stage, the preform is drawn into a fiber using a precision-feed mechanism that feeds it into a furnace at a proper speed. During this process, the relative core-cladding dimensions are preserved. Both stages, preform fabrication and fiber drawing, involve sophisticated technology to ensure the uniformity of the core size and the index profile.

Several methods can be used for making a preform. The three commonly used methods are modified chemical vapor deposition (MCVD), outside vapor deposition (OVD), and vapor-phase axial deposition (VAD). Figure 9.6 shows a schematic diagram of the MCVD process. In this process, successive layers of SiO_2 are deposited on the inside of a fused silica tube by mixing the vapors of $SiCl_4$ and O_2 at a temperature of $\approx 1800^{\circ}C$. To ensure uniformity, the multiburner torch is moved back and forth across the tube length. The refractive index of the cladding layers is controlled by adding fluorine to the tube. When a sufficient cladding thickness has been deposited with multiple passes of the torch, the vapors of $GeCl_4$ or $GeCl_3$ are added to the vapor mixture

to form the core. When all layers have been deposited, the torch temperature is raised to collapse the tube into a solid rod known as the preform.

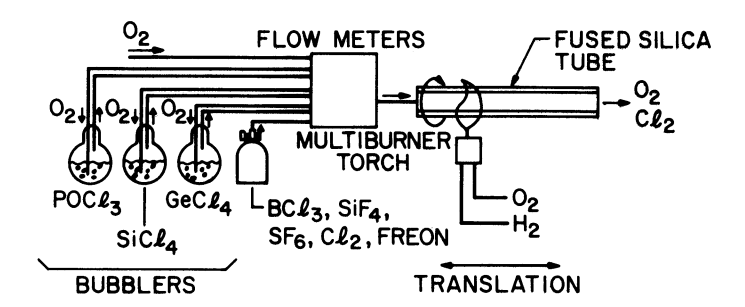


Figure 9.6: Schematic diagram of the MCVD process commonly used for fiber fabrication.

This description is extremely brief and is intended to provide a general idea. The fabrication of optical fibers requires attention to a large number of technological details. The interested reader is referred to the extensive literature on this subject.

Fiber Losses

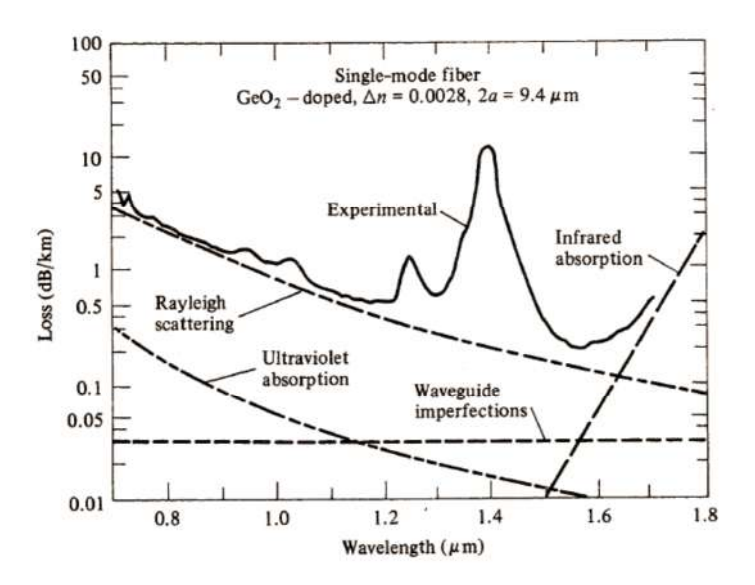


Figure 9.7: Fiber Absorption Spectrum

An important fiber parameter is a measure of power loss during transmission of optical signals inside the fiber. If P_0 is the power launched at the input of a fiber of length L, the transmitted power P_T is given by

$$P_T = P_0 e^{-\alpha L} \tag{9.1.3}$$

where the attenuation constant α is a measure of total fiber losses from all sources. It is customary to express in units of dB/km using the relation

$$\alpha_{\rm dB} = \frac{10}{L} \log \left(\frac{P_T}{P_0} \right) = 4.343\alpha \tag{9.1.4}$$

where Eq. (9.1.3) was used to relate $\alpha_{\rm dB}$ and α .

As one may expect, fiber losses depend on the wavelength of light. Figure 9.7 shows the loss spectrum of a silica fiber made by the MCVD process. This fiber exhibits a minimum loss of about 0.2 dB/km near 1.55 μ m. Losses are considerably higher at shorter wavelengths, reaching a level

of a few dB/km in the visible region. Note, however, that even a 10-dB/km loss corresponds to an attenuation constant of only $\alpha \approx 2 \times 10^{-5}$ cm⁻¹, an incredibly low value compared to that of most other materials.

Several factors contribute to the loss spectrum of Fig. 9.7, with material absorption and Rayleigh scattering contributing dominantly. Silica glass has electronic resonances in the ultraviolet (UV) region and vibrational resonances in the far-infrared (FIR) region beyond 2 μ m but absorbs little light in the wavelength region 0.52 μ m. However, even a relatively small amount of impurities can lead to significant absorption in that wavelength window. From a practical point of view, the most important impurity affecting fiber loss is the OH ion, which has a fundamental vibrational absorption peak at $\approx 2.73 \mu$ m. The overtones of this OH-absorption peak are responsible for the dominant peak seen in Fig. 9.7 near 1.4 μ m and a smaller peak near 1.23 μ m. Special precautions are taken during the fiber-fabrication process to ensure an OH-ion level of less than one part in one hundred million. In state-of-the-art fibers, the peak near 1.4 μ m can be reduced to below the 0.5-dB level. It virtually disappears in especially prepared fibers. Such fibers with low losses in the entire 1.31.6 μ m spectral region are useful for fiber-optic communications and were available commercially by the year 2000 (e.g., all-wave fiber).

Rayleigh scattering is a fundamental loss mechanism arising from density fluctuations frozen into the fused silica during manufacture. Resulting local fluctuations in the refractive index scatter light in all directions. The Rayleighscattering loss varies as λ^{-4} and is dominant at short wavelengths. As this loss is intrinsic to the fiber, it sets the ultimate limit on fiber loss. The intrinsic loss level (shown by a dashed line in Fig. 9.7) is estimated to be (in dB/km)

$$\alpha_R = C_R / \lambda^4 \tag{9.1.5}$$

where the constant C_R is in the range 0.70.9 dB/(km- μ m⁴) depending on the constituents of the fiber core. As $\alpha_R = 0.120.15$ dB/km near $\lambda = 1.55\mu$ m, losses in silica fibers are dominated by Rayleigh scattering. In some glasses, α_R can be reduced to a level ~ 0.05 dB/km. Such glasses may be useful for fabricating ultra low-loss fibers.

Among other factors that may contribute to losses are bending of fiber and scattering of light at the core-cladding interface. Modern fibers exhibit a loss of ≈ 0.2 dB/km near 1.55 μ m. Total loss of fiber cables used in optical communication systems is slightly larger (by ~ 0.03 dB/km) because of splice and cabling losses.

Chromatic Dispersion

When an electromagnetic wave interacts with the bound electrons of a dielectric, the medium response, in general, depends on the optical frequency ω . This property, referred to as chromatic dispersion, manifests through the frequency dependence of the refractive index $n(\omega)$. On a fundamental level, the origin of chromatic dispersion is related to the characteristic resonance frequencies at which the medium absorbs the electromagnetic radiation through oscillations of bound electrons. Far from the medium resonances, the refractive index is well approximated by the Sellmeier equation

$$n^{2}(\omega) = 1 + \sum_{j=1}^{m} \frac{B_{j}\omega_{j}^{2}}{\omega_{j}^{2} - \omega^{2}}$$
(9.1.6)

where ω_j is the resonance frequency and B_j is the strength of jth resonance. The sum in Eq. (9.1.6) extends over all material resonances that contribute to the frequency range of interest. In the case of optical fibers, the parameters B_j and ω_j are obtained experimentally by fitting the measured dispersion curves to Eq. (9.1.6) with m=3 and depend on the core constituents. For bulk-fused silica, these parameters are found to be $B_1=0.6961663, B_2=0.4079426, B_3=0.8974794, \lambda_1=0.0684043 \mu m$, $\lambda_2=0.1162414 \mu m$, and $\lambda_3=9.896161 \mu m$, where $\lambda_j=2\pi c/\omega_j$ and c is the speed of light in vacuum.

Fiber dispersion plays a critical role in propagation of short optical pulses because different spectral components associated with the pulse travel at different speeds given by $c/n(\omega)$. Even when the nonlinear effects are not important, dispersion-induced pulse broadening can be detrimental for optical communication systems. In the nonlinear regime, the combination of dispersion and

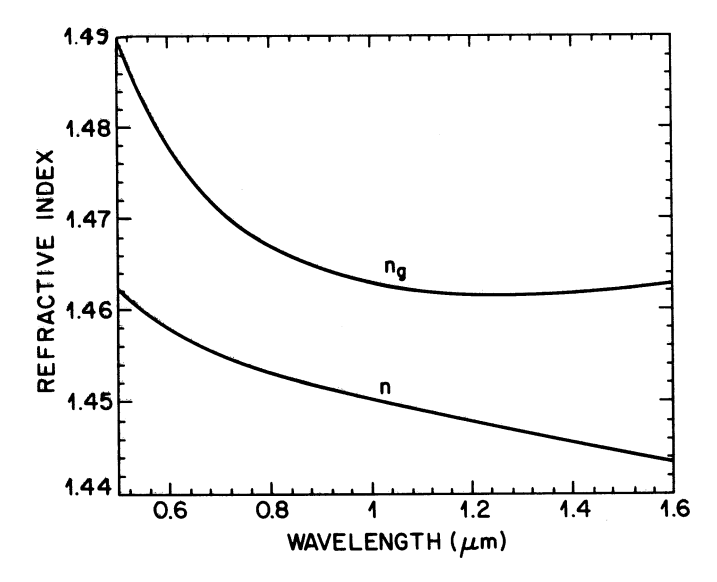


Figure 9.8: Variation of refractive index n and group index n_q with wavelength for fused silica.

nonlinearity can result in a qualitatively different behavior, as discussed in later chapters. Mathematically, the effects of fiber dispersion are accounted for by expanding the mode-propagation constant β in a Taylor series about the frequency ω_0 at which the pulse spectrum is centered:

$$\beta(\omega) = n(\omega)\frac{\omega}{c} = \beta_0 + \beta_1(\omega - \omega_0) + \frac{1}{2}\beta_2(\omega - \omega_0)^2 + \dots$$
 (9.1.7)

where

$$\beta_m = \left(\frac{d^m \beta}{d\omega^m}\right)_{(i)=(i)} \qquad (m = 0, 1, 2, \dots)$$
(9.1.8)

The parameters β_1 and β_2 are related to the refractive index n and its derivatives through the relations

$$\beta_1 = \frac{1}{v_g} = \frac{n_g}{c} = \frac{1}{c} \left(n + \omega \frac{dn}{d\omega} \right) \tag{9.1.9}$$

$$\beta_2 = \frac{1}{c} \left(2 \frac{dn}{d\omega} + \omega \frac{d^2 n}{d\omega^2} \right) \tag{9.1.10}$$

where n_g is the group index and v_g is the group velocity. Physically speaking, the envelope of an optical pulse moves at the group velocity while the parameter β_2 represents dispersion of the group velocity and is responsible for pulse broadening. This phenomenon is known as the group-velocity dispersion (GVD), and β_2 is the GVD parameter.

Figures 9.8 and 9.9 show how n, n_g , and β_2 vary with wavelength λ in fused silica using Eqs. (9.1.6), (9.1.9), and (9.1.10). The most notable feature is that β_2 vanishes at a wavelength of about 1.27 μ m and becomes negative for longer wavelengths. This wavelength is referred to as the zero-dispersion wavelength and is denoted as λ_D . However, note that dispersion does not vanish at $\lambda = \lambda_D$. Pulse propagation near this wavelength requires inclusion of the cubic term in Eq. (9.1.7). The coefficient β_3 appearing in that term is called the third-order dispersion (TOD) parameter. Such higher-order dispersive effects can distort ultrashort optical pulses both in the linear and nonlinear regimes. Their inclusion is necessary only when the wavelength λ approaches λ_D to within a few nanometers.

The curves shown in Figs. 9.8 and 9.9 are for bulk-fused silica. The dispersive behavior of actual glass fibers deviates from that shown in these figures for the following two reasons. First, the fiber core may have small amounts of dopants such as GeO_2 and P_2O_5 . Equation (9.1.6) in that case should be used with parameters appropriate to the amount of doping levels. Second, because

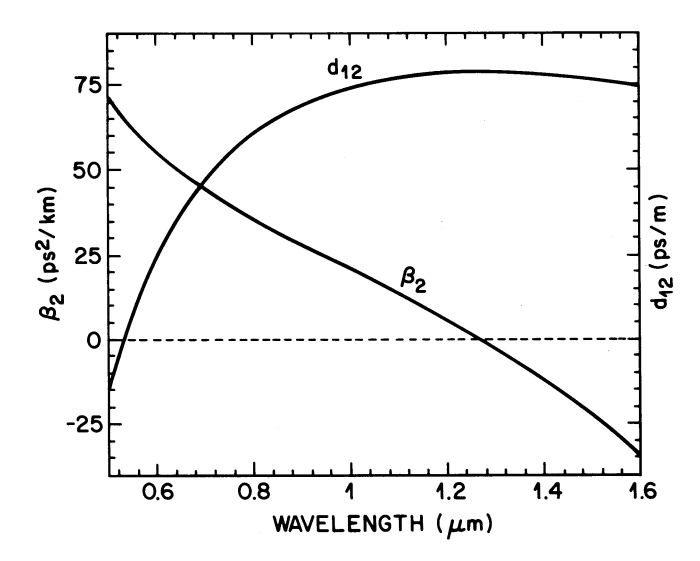


Figure 9.9: Variation of β_2 and d_{12} with wavelength for fused silica. The dispersion parameter $\beta_2 = 0$ near 1.27 μ m.

of dielectric waveguiding, the effective mode index is slightly lower than the material index $n(\omega)$ of the core, reduction itself being ω dependent. This results in a waveguide contribution that must be added to the material contribution to obtain the total dispersion. Generally, the waveguide contribution to β_2 is relatively small except near the zero-dispersion wavelength λ_D where the two become comparable. The main effect of the waveguide contribution is to shift λ_D slightly toward longer wavelengths; $\lambda_D \approx 1.31 \mu \text{m}$ for standard fibers. Figure 9.10 shows the measured total dispersion of a singlemode fiber. The quantity plotted is the dispersion parameter D that is commonly used in the fiber-optics literature in place of β_2 . It is related to β_2 by the relation

$$D = \frac{d\beta_1}{d\lambda} = -\frac{2\pi c}{\lambda^2} \beta_2 \approx \frac{\lambda}{c} \frac{d^2 n}{d\lambda^2}$$
 (9.1.11)

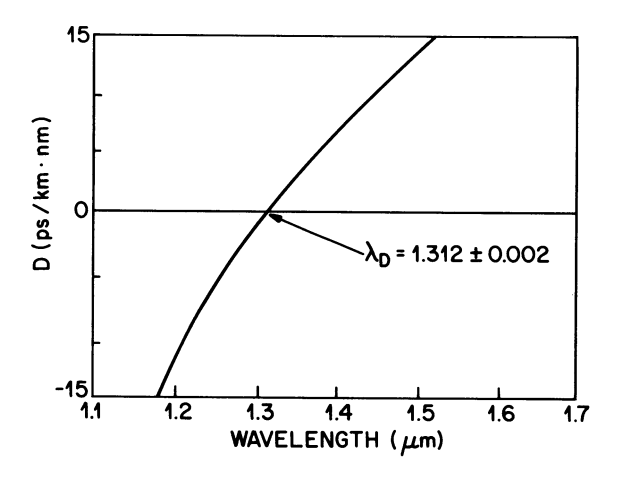


Figure 9.10: Measured variation of dispersion parameter D with wavelength for a single-mode fiber.

An interesting feature of the waveguide dispersion is that its contribution to D (or β_2) depends on fiber-design parameters such as core radius a and core-cladding index difference Δ . This feature can be used to shift the zero dispersion wavelength λ_D in the vicinity of 1.55 μ m where the fiber loss is minimum. Such dispersion-shifted fibers have found applications in optical communication

systems. They are available commercially and are known by names such as zero- and nonzerodispersion-shifted fibers, depending on whether $D \approx 0$ at 1.55 μ m or not. Those fibers in which GVD is shifted to the wavelength region beyond 1.6 μ m exhibit a large positive value of β_2 . They are called dispersion-compensating fibers (DCFs). The slope of the curve in Fig. 9.10 (called the dispersion slope) is related to the TOD parameter β_3 . Fibers with reduced slope have been developed in recent years for wavelengthdivision- multiplexing (WDM) applications.

It is possible to design dispersion-flattened optical fibers having low dispersion over a relatively large wavelength range 1.31.6 μm . This is achieved by using multiple cladding layers. For comparison, dispersion of a single-clad fiber is also shown by a dashed line. The quadruply clad fiber has low dispersion ($|D| \sim 1$ ps/km-nm) over a wide wavelength range extending from 1.25 to 1.65 μm . Waveguide dispersion can also be used to make fibers for which D varies along the fiber length. An example is provided by dispersion-decreasing fibers made by tapering the core diameter along the fiber length.

Nonlinear effects in optical fibers can manifest qualitatively different behaviors depending on the sign of the GVD parameter. For wavelengths such that $\lambda < \lambda_D$, the fiber is said to exhibit normal dispersion as $\beta_2 > 0$ (see Fig. 9.9). In the normal-dispersion regime, high-frequency (blue-shifted) components of an optical pulse travel slower than low-frequency (red-shifted) components of the same pulse. By contrast, the opposite occurs in the anomalous dispersion regime in which $\beta_2 < 0$. As seen in Fig. 9.9, silica fibers exhibit anomalous dispersion when the light wavelength exceeds the zero-dispersion wavelength $(\lambda > \lambda_D)$. The anomalous-dispersion regime is of considerable interest for the study of nonlinear effects because it is in this regime that optical fibers support solitons through a balance between the dispersive and nonlinear effects.

An important feature of chromatic dispersion is that pulses at different wavelengths propagate at different speeds inside a fiber because of a mismatch in their group velocities. This feature leads to a walk-off effect that plays an important role in the description of the nonlinear phenomena involving two or more closely spaced optical pulses. More specifically, the nonlinear interaction between two optical pulses ceases to occur when the faster moving pulse completely walks through the slower moving pulse. This feature is governed by the walk-off parameter d_{12} defined as

$$d_{12} = \beta_1(\lambda_1) - \beta_1(\lambda_2) = v_q^{-1}(\lambda_1) - v_q^{-1}(\lambda_2)$$
(9.1.12)

where λ_1 and λ_2 are the center wavelengths of two pulses and β_1 at these wavelengths is evaluated using Eq. (9.1.9). For pulses of width T_0 , one can define the walk-off length L_W by the relation

$$L_W = T_0/|d_{12}| (9.1.13)$$

Figure 9.9 shows variation of d_{12} with λ_2 for fused silica using Eq. (9.1.12) with $\lambda_1=0.532\mu\mathrm{m}$. In the normal-dispersion regime ($\beta_2>0$), a longerwavelength pulse travels faster, while the opposite occurs in the anomalous dispersion region. For example, if a pulse at $\lambda_2=1.06\mu\mathrm{m}$ copropagates with the pulse at $\lambda_1=0.532\mu\mathrm{m}$, it will separate from the shorter-wavelength pulse at a rate of about 80 ps/m. This corresponds to a walk-off length L_W of only 25 cm for $T_0=20$ ps. The group-velocity mismatch plays an important role for nonlinear effects involving cross-phase modulation

9.2 Optical fiber and single mode fibers ³

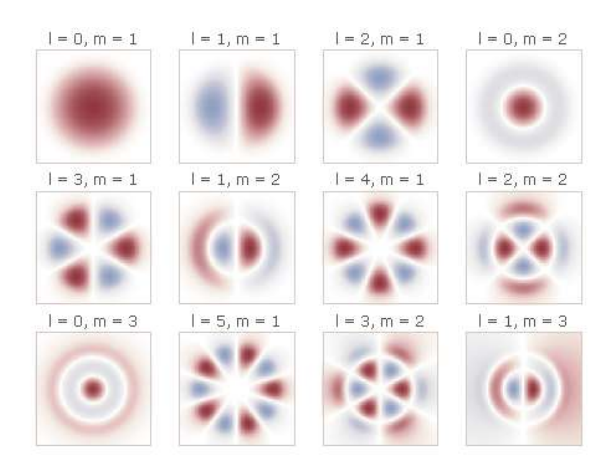


Figure 9.11: Different modes in fiber.

The theory of the guided propagation of light in optical fibers is straightforward conceptually but somewhat complicated in its algebraic details, which we will largely skip over; the interested reader will not find it difficult to fill in at least some of the steps, or to find comprehensive discussions and references in more specialized books.⁴

Optical fibers guide light by total internal reflection. Figure 9.12 is an enlarged view of a segment of an optical fiber; the core diameter may be as small as a few microns, as explained below. The critical angle for total internal reflection is

$$\theta_c = \sin^{-1}\left(\frac{n_2}{n_1}\right) \tag{9.2.1}$$

where n_2 and n_1 are the refractive indices of the cladding and the core, respectively (Fig. 9.12).

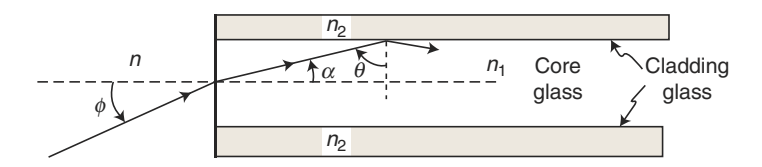


Figure 9.12: An optical fiber, viewed along a direction perpendicular to the fiber axis.

Total internal reflection occurs for angles of incidence $\theta \geq \theta_c$. This implies a maximum "acceptance angle" for which light injected into the fiber will undergo total internal reflection. Applying Snells law to the dielectric interface at the entrance to the fiber in Fig. 9.12, we have

$$n\sin\phi = n_1\sin\alpha = n_1\sin(\frac{\pi}{2} - \theta) = n_1\cos\theta = n_1\sqrt{1 - \sin^2\theta}$$
(9.2.2)

For $\theta = \theta_c$,

$$n\sin\phi = n_1\sqrt{1 - \frac{n_2^2}{n_1^2}} = \sqrt{n_1^2 - n_2^2} \equiv \text{NA}$$
 (9.2.3)

where the number NA is called the numerical aperture of the fiber. According to these equations the angle

$$\phi_{\text{max}} = \sin^{-1}\left(\frac{\text{NA}}{n}\right) \tag{9.2.4}$$

 $^{^3{\}rm Chapter~8}$ (Pages 355 - 364) - Laser Physics - Peter W. Milonni, Joseph H. Eberly - Hoboken, New Jersey : John Wiley & Sons Ltd, 2010

⁴See, for instance, G. P. Agrawal, Fiber-Optic Communication Systems, 3rd ed., Wiley, New York, 2002, and references therein.

is the maximum acceptance angle at which there is total internal reflection. For a fiber in air $(n \cong 1)$ with a core refractive index $n_1 = 1.53$ and a cladding index $n_2 = 1.50$, NA = 0.3 and the maximum acceptance angle is $\phi_{\text{max}} \cong 18^{\circ}$. As in this example, the difference between n_1 and n_2 is typically only a few percent, and so one conventionally introduces the small parameter $\Delta = (n_1 - n_2)/n_1$, in terms of which

$$NA = \sqrt{n_1 \Delta (n_1 + n_2)} \cong n_1 \sqrt{2\Delta}$$
(9.2.5)

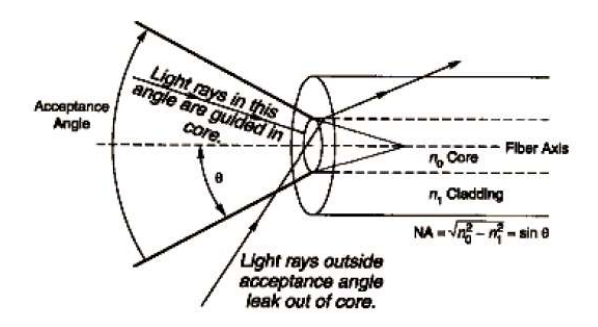


Figure 9.13: Acceptance angle of fiber.

The numerical aperture is obviously a measure of the amount of light that can be taken in and guided by the fiber. However, fibers with large numerical apertures have disadvantages for communication purposes because they admit a large number of propagation modes and therefore suffer from an effect known as intermodal dispersion. We discussed in the preceding section the material dispersion associated with the frequency dependence of the refractive index, but in fibers there is also a pulse-broadening effect associated with different angles of incidence θ in Fig. 9.12. Since different angles are associated with different modes of propagation, this dispersive effect is called intermodal. To estimate the pulse broadening due to intermodal dispersion, consider the propagation paths for two pulses, one propagating along the core axis and the other having an angle of incidence u at the corecladding interface (Fig. 9.12). For a fiber length L the off-axis pulse has a total propagation length $L/\cos\alpha$, whereas the propagation length for the on-axis pulse is simply L. These different propagation paths imply a difference ΔT in the propagation times for pulses with group velocity v_g to reach the end of the fiber. For the lowest-order modes of a fiber it is found that $v_g \cong c/n_1$, the phase velocity in the core. Thus,

$$\Delta T \cong L \frac{(1/\cos\alpha) - 1}{c/n_1} \cong \frac{n_1\alpha^2 L}{2c}$$
(9.2.6)

where the angle α is assumed to be very small. For the maximum acceptance angle defined by (9.2.4), it follows from (9.2.2) that $n_1 \sin \alpha = \text{NA}$, or $\alpha = \text{NA}/n_1$ in the small-angle approximation. Then (9.2.6) becomes

$$\Delta T \cong \frac{(\text{NA})^2}{2n_1c}L\tag{9.2.7}$$

for these two modes. A multimode pulse will therefore undergo a temporal broadening.

Intermodal dispersion is reduced when the fiber is of the graded-index type rather than the step-index type illustrated in Fig. 9.12. In a graded-index fiber the refractive index does not have a sharp, steplike decrease from n_1 to n_2 . Instead the index decreases more smoothly from the center of the fiber. An index distribution that is frequently used in practice is described by the formula

$$n^2 = n_c^2 (1 - a_2^2 r^2) (9.2.8)$$

where n_c is the refractive index at the center, r is the distance from the center, and a_2^2 is a constant. The advantage of a graded-index fiber is a consequence of the following result, which we will not take the time to derive: The temporal spread ΔT for a graded-index fiber is proportional to $(NA)^4$ rather than to $(NA)^2$ as in the step-index case. Thus, a small numerical aperture implies smaller

intermodal dispersion in a graded-index fiber than in a step-index fiber. It is easy to understand physically why this is so. In the graded-index case the light rays along the axis of the fiber travel a shorter path than off-axis rays but have a smaller phase velocity because of the larger index on-axis [Eq. (9.2.8)]. The graded index therefore reduces the difference in propagation times of different modes.

Intermodal dispersion is completely absent in a *single-mode fiber*. We now consider in more detail the propagation modes of an optical fiber.

For laser resonators we defined a mode as a field distribution that does not change in form upon back-and-forth propagation in the resonator. In the case of an optical fiber, similarly, we define a mode as a field distribution that retains its form during propagation in the fiber. Thus,we require that the electric field satisfy the Helmholtz equation, with the refractive index having the spatial distribution appropriate to the fiber under consideration. In addition to satisfying Helmholtz equation, the field must, of course, satisfy the appropriate boundary conditions. We will consider a step-index fiber with $n = n_1$ for $r \le a$ and $n = n_2$ for r > a (Fig. 9.14).

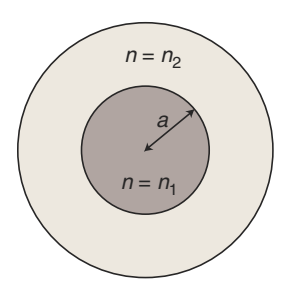


Figure 9.14: Cross-sectional view of a step-index fiber.

The fiber geometry obviously suggests the use of cylindrical coordinates (r, ϕ, z) , in terms of which Helmholtz equation takes the form

$$\frac{\partial^2 E}{\partial r^2} + \frac{1}{r} \frac{\partial E}{\partial r} + \frac{1}{r^2} \frac{\partial^2 E}{\partial \phi^2} + \frac{\partial^2 E}{\partial z^2} + n^2 \frac{\omega^2}{c^2} E = 0$$
 (9.2.9)

Since a rotation by 2π about the fiber axis cannot affect the field, a solution of (9.2.9) must not change when 2π is added to ϕ . Thus, E must vary with ϕ as $e^{im\phi}$, where $m = 0, \pm 1, \pm 2, \ldots$ We seek solutions describing propagation along the z axis, and therefore write⁵

$$E(r,\phi,z) = F(r)e^{im\phi}e^{i\beta z} \tag{9.2.10}$$

where the propagation constant β is at this point unspecified. Such a field retains its form except for a phase factor $[e^{i\beta z}]$, and therefore defines a mode of the fiber. Using this form in (9.2.9), we obtain for the radial function F(r) the ordinary differential equation

$$\frac{d^2F}{dr^2} + \frac{1}{r}\frac{dF}{dr} + \left(n^2\frac{\omega^2}{c^2} - \beta^2 - \frac{m^2}{r^2}\right)F = 0$$
 (9.2.11)

Thus, in the core region,

$$\frac{d^2F}{dr^2} + \frac{1}{r}\frac{dF}{dr} + \left(k^2 - \frac{m^2}{r^2}\right)F = 0 \qquad (r \le a)$$
 (9.2.12)

where

$$\kappa^2 = n_1^2 \frac{\omega^2}{c^2} - \beta^2 \equiv n_1^2 k_0^2 - \beta^2 \tag{9.2.13}$$

Equation (9.2.12) has the form of the Bessel differential equation. The solutions that remain finite as $r \to 0$ are the Bessel functions $J_m(\kappa r)$ of the first kind, which we have already used in the preceding chapter

$$F(r) = AJ_m(\kappa r) \qquad (r \le a) \tag{9.2.14}$$

 $^{^{5}\}mathrm{We}$ are employing here the method of separation of variables

where A is a constant.

In the cladding region we write

$$\frac{d^2F}{dr^2} + \frac{1}{r}\frac{dF}{dr} + \left(\gamma^2 - \frac{m^2}{r^2}\right)F = 0 \qquad (r > a)$$
 (9.2.15)

where

$$\gamma^2 = \beta^2 - n_2^2 \frac{\omega^2}{c^2} \equiv \beta^2 - n_2^2 k_0^2 \tag{9.2.16}$$

We assume that γ^2 is positive, that is, that γ is real, in order to have solutions for r > a that go to 0 as $r \to \infty$. These solutions are of the form

$$F(r) = BK_m(\gamma r) \qquad (r > a) \tag{9.2.17}$$

where K_m is a modified Bessel function of the second kind. Plots of $J_m(x)$ and $K_m(x)$ are readily found in various handbooks or on the Web. For our purposes at this point we need only know that $J_m(\kappa r)$ is finite at r=0 and that $K_m(\gamma r) \to 0$ as $r \to \infty$, which are necessary conditions if the solutions (9.2.15) and (9.2.17) are to be applicable in the core and cladding regions, respectively.

We have not invoked here the paraxial approximation. In fact, the solutions given by (9.2.10) and (9.2.14) for the field in the core are of the same form as the (nonparaxial) Bessel beam modes of free space, except that here the propagation is in a medium with refractive index n_1 rather than free space, and the propagation constant β is fixed by the fact that the tangential components of the field must be continuous at the corecladding interface. In the case of a fiber the paraxial approximation may not be a good one because the field is guided by total internal reflection and, depending on the difference $n_1 - n_2$, the angles that rays make with respect to the fiber axis are not necessarily small.

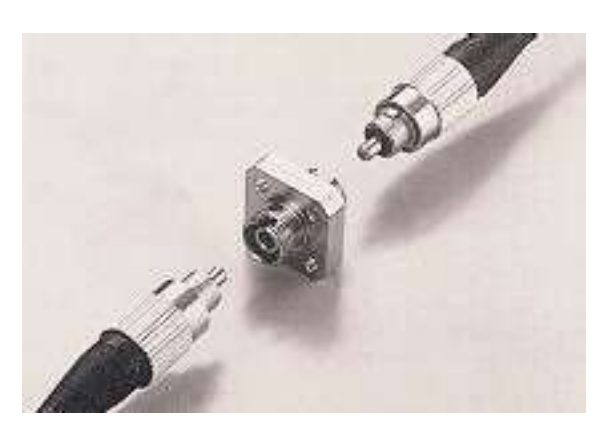


Figure 9.15: Fiber optics components (Cabled fibers and connector)

The Helmholtz equation applies to a single component of the electric field envelope E, and also to a single component of the slowly varying magnetic field envelope H. Given E_z and H_z , for instance, we can obtain E_x, E_y, H_x , and H_y from the Maxwell equations

$$\nabla \times \mathbf{E} = i\omega \mu_0 \mathbf{H} \tag{9.2.18}$$

$$\nabla \times \mathbf{H} = -i\omega \mu_0 \mathbf{E} = -i\omega n^2 \epsilon_0 \mathbf{E} \tag{9.2.19}$$

for a field that varies with time as $e^{-i\omega t}$ and with z as $e^{i\beta z}$. Consider, for example, the component H_x of **H**. From (9.2.18),

$$i\omega\mu_0 H_x = \frac{\partial E_z}{\partial y} - \frac{\partial E_y}{\partial z} = \frac{\partial E_z}{\partial y} - i\beta E_y$$
 (9.2.20)

and, from (9.2.19),

$$E_y = \frac{i}{\omega n^2 \epsilon_0} \left(-\frac{\partial H_z}{\partial x} + \frac{\partial H_x}{\partial z} \right) \tag{9.2.21}$$

Using (9.2.21) in (9.2.20), and $\epsilon_0 \mu_0 = 1/c^2$, we obtain for the core region $(n^2 = n_1^2)$

$$H_x = -\frac{i}{\kappa^2} \left(\omega n_1^2 \epsilon_0 \frac{\partial E_z}{\partial y} - \beta \frac{\partial H_z}{\partial x} \right) \tag{9.2.22}$$

In the same fashion we obtain, in both the core and cladding regions, E_x, E_y , and H_x, H_y in terms of E_z and H_z . Of course, we can express this as well in terms of cylindrical components of the slowly varying envelope functions: We can express E_r, E_ϕ, H_r , and H_ϕ in terms of E_z and H_z satisfying

$$E_z(r,\phi,z) = AJ_m(\kappa r)e^{im\phi}e^{i\beta z}$$
(9.2.23a)

$$H_z(r,\phi,z) = BJ_m(\kappa r)e^{im\phi}e^{i\beta z}$$
(9.2.23b)

for $r \leq a$ and

$$E_z(r,\phi,z) = CK_m(\gamma r)e^{im\phi}e^{i\beta z}$$
(9.2.24a)

$$H_z(r,\phi,z) = DK_m(\gamma r)e^{im\phi}e^{i\beta z}$$
(9.2.24b)

for r > a.

Maxwells equations require that the tangential components of ${\bf E}$ and ${\bf H}$ be continuous at the correctly correctly continuous at r=a. That is, E_z, E_ϕ, H_z , and H_ϕ must be continuous at r=a. Requiring this continuity leads to four homogeneous linear algebraic equations for the constants A, B, C, and D appearing in Eqs. (9.2.23), i.e., equations of the form $a_{1i}A + a_{2i}B + a_{3i}C + a_{4i}D = 0$, j=1,2,3,4. In order for these equations to have non vanishing solutions for A,B,C, and D, the determinant of the coefficient matrix (a_{ij}) , i, j = 1, 2, 3, 4, must vanish. This requirement takes the form of a complicated equation involving $J_m(\kappa a), J'_m(\kappa a), K_m(\gamma a)$, and $K'_m(\gamma a)$, where the primes denote derivatives. This "characteristic equation," which must be solved numerically, determines the propagation constant β for given values of ω , a, n_1 , and n_2 , that is, for a given frequency ω and for a given core radius a and core and cladding refractive indices n_1 and n_2 , respectively.

For given values of ω , a, and n_1, n_2 , the values of β determined by the numerical solution of the characteristic equation will depend on the integer m. For each m there is in general more than one solution for β ; these different solutions can be denoted $\beta_m, j = 1, 2, 3, \ldots$, and each β_{mj} defines a mode of the fiber. That is, a mode is defined by the pair of integers m and j that specify the spatial dependence of the electric and magnetic fields. The electric and magnetic fields for each mode are defined by Eqs. (9.2.23) and the equations relating the other field components to E_z and H_z , with κ and γ depending on β_{mj} [Eq. (9.2.13) and (9.2.16)].

We are interested in guided modes in which the electric and magnetic fields fall off with radial distance from the fiber. Consider the fields (9.2.23) for $\gamma r \gg 1$. In this limit

$$K_m(\gamma r) \approx \left(\frac{\pi}{2\gamma r}\right)^{1/2} \left(1 - \frac{4m^2 - 1}{8\gamma r}\right) e^{-\gamma r}$$
(9.2.25)

and the electric and magnetic fields (9.2.23) for a mode characterized by this radial dependence decay exponentially with distance from the fiber if γ is real ($\gamma^2 > 0$). If γ is purely imaginary $(\gamma^2 < 0)$, however, the mode is not "guided"; the exponential decay of (9.2.24) is replaced by $e^{-i|\gamma|r} = \cos|\gamma|r - i\sin|\gamma|r$ for $\gamma = i|\gamma|$. Therefore, $\gamma^2 = 0$ defines the "cut-off" between guided and unguided modes: $\gamma^2 > 0$ implies a guided mode, whereas $\gamma^2 < 0$ implies an unguided mode. From (9.2.13) and (9.2.16) we see that $\gamma^2 = 0$ implies that $\kappa = k_0 \sqrt{n_1^2 - n_2^2}$. The dimensionless

"V parameter,"

$$V = k_0 a \sqrt{n_1^2 - n_2^2} = \frac{\omega}{c} a \sqrt{n_1^2 - n_2^2} = \frac{\omega a}{c} \text{NA},$$
(9.2.26)

determines the number of modes: fibers with large V parameters have many modes as determined by numerical solutions of the characteristic equation. The number of modes is found to be approximately $V^2/2$ for $V \gg 1$. But if V is made small enough, it is found that only the fundamental mode with m=0 is guided by the fiber. Such single-mode fibers are of special interest for communication systems, and we will therefore devote the following section to them

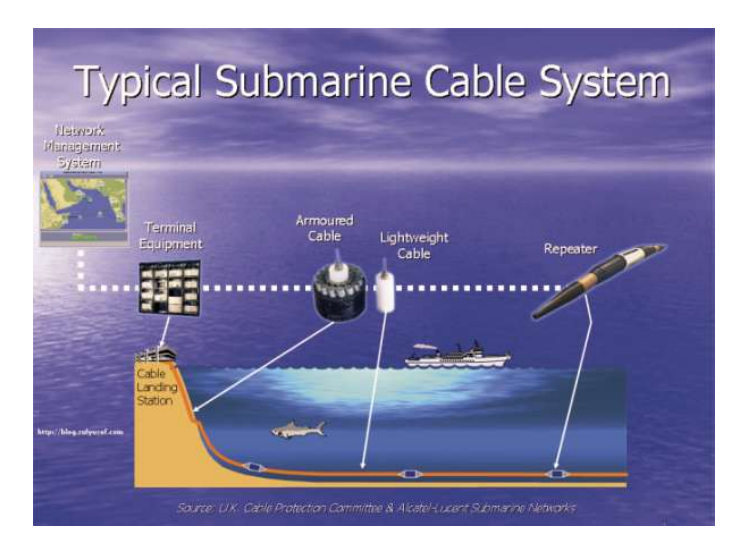


Figure 9.16: Typical submarine fiber system

SINGLE-MODE FIBERS

In the preceding section we noted that the requirement that E_z, E_π, H_z , and H_ϕ be continuous at the corecladding interface leads to a complicated characteristic equation involving $J_m(\kappa a), J'_m(\kappa a), K_m(\gamma a)$, and $K'_m(\gamma a)$. Numerical solutions of this equation determine the guided modes of the fiber for real values of the parameter γ defined by (9.2.16). Analysis of the characteristic equation shows that when $V < V_c$, where V_c is defined as the smallest value of V satisfying $J_0(V) = 0$, the fiber supports only the single mode with m = 0; there are no other guided modes for $V < V_c$.

The smallest "zero" of $J_0(x)$, that is, the smallest x such that $J_0(x) = 0$, is approximately 2.405. Thus, a step-index fiber will support only a single mode when $V_c < 2.405$, or in other words when

$$\frac{\omega}{c}a\sqrt{n_1^2 - n_2^2} = \frac{2\pi a}{\lambda} \text{NA} < 2.405$$
 (9.2.27)

For $\lambda=2\pi c/\omega=1.3\mu\mathrm{m}$, $n_1=1.450$, and $n_2=1.443$, this single-mode condition is satisfied if the core radius $a<3.5\mu\mathrm{m}$. These values are in the range characteristic of the single-mode fibers used in communication systems. Obviously, the single-mode condition can be satisfied if the wavelength is large enough or if the core diameter and the numerical aperture are small enough.

In order to realize the single-mode condition (9.2.27) for wavelengths of interest and for core diameters that are not unreasonably small, the numerical aperture NA = $\sqrt{n_1^2 - n_2^2}$ be small. Fibers typically have values of $\Delta = (n_1 - n_2)/n_1 \approx 0.01$ and, as noted in the preceding section, the guided modes in this case are approximately paraxial, with z components of the field small compared to the transverse (x and y) components. That is, the guided modes are approximately transverse, and a linearly polarized mode has an electric field component of the form

$$E_x(r,\phi,z) = E_x(r,z) = E_0 \frac{J_0(\kappa r)}{J_0(\kappa a)} e^{i\beta z} \qquad (r \le a)$$

$$= E_0 \frac{K_0(\gamma r)}{K_0(\gamma a)} e^{i\beta z} \qquad (r > a) \qquad (9.2.28)$$

where E_0 is a constant specifying the amplitude of the field at r = a. The function $J_0(x)$ peaks at x = 0 ($J_0(0) = 1$) and its falloff to 0 at x = 2.405... follows roughly a bell shaped curve, while the variation of $K_0(x)$ for large values of x is given by (9.2.24). The field (9.2.28) for a single-mode fiber is therefore often approximated by a Gaussian function:

$$E_x(r,z) \approx E_0 e^{-r^2/w^2} e^{i\beta z} \tag{9.2.29}$$

where the spot size w depends on the V parameter of the fiber and is $\cong a$ for $V \cong 2$. Thus, the single guided modes of fibers of interest for optical communication systems are approximately paraxial, transverse, and Gaussian, with a spot size on the order of the core diameter.

• The calculation and characterization of the modes of an optical fiber are obviously rather complicated, and it is beyond our scope to delve much further into the subject. A few more general remarks, however, are appropriate.

The astute reader will have noticed that we have in effect assumed an infinite cladding region. The justification for this assumption is the exponential decay of the electric and magnetic fields of the guided modes outside the core [Eq. (9.2.24)]. Optical fibers are in fact designed so that the fields are negligibly small at the outer surface of the cladding. If this were not the case, light would be lost due to scattering from surface irregularities on the outer surface of the fiber.

As already noted, the core and cladding refractive indices in optical fibers typically differ by only a few percent. The critical angle for total internal reflection is therefore relatively large, making the guided modes approximately paraxial and the z components of the electric and magnetic fields small in magnitude compared to the transverse components. Each (m, j) mode is then approximately transverse and we can associate with it two "degenerate" orthogonal linear polarizations having the same (r, ϕ, z) dependence. If the fiber cross section were perfectly circular, a linearly polarized field would maintain its polarization, but in reality there are always slight imperfections in the core diameter, for instance, that cause the fiber to be birefringent in the sense that the mode index β/k_0 is different for the two orthogonally polarized modes. A "single-mode" fiber will have two mode indices, \bar{n}_x and \bar{n}_y , and this causes the two orthogonal polarizations to exchange power. In practice, the injection of a linearly polarized field into the fiber results in an output field whose polarization is unpredictable as a consequence of random fluctuations of the birefringence. In polarization preserving fibers a relatively large and deterministic birefringence is introduced to overcome the random birefringence

The major breakthroughs that led to the widespread use of optical fibers in communication systems were the development of fibers with low attenuation and of compact (diode) lasers for efficiently coupling light into fibers. In the early 1970s fibers were developed at Corning Glass Works with attenuations $A \sim 20 dB/km$ at wavelengths around 1 μ m, compared to attenuations $\sim 1000 dB/km$ characteristic of the fibers manufactured earlier. The fused silica currently used to make optical fibers absorbs in the ultraviolet as a consequence of electronic resonances of the SiO₂ molecules and in the infrared as a consequence of molecular vibrations. The ultraviolet and infrared absorption together produce a broad absorption spectrum with A < 0.03 dB/km in the wavelength range 1.3 - 1.6 μ m used in fiber-optic communications, and with an absorption minimum at 1.55 μ m. Water vapor and, to a lesser extent, metallic impurities, are the dominant sources of absorption losses in silica fibers, and these losses, together with the loss due to Rayleigh scattering from local density fluctuations, exceed the intrinsic absorption loss of pure silica. All the sources of power loss in currently manufactured telecommunication fibers combine to produce an attenuation minimum of about 0.2 dB/km at 1.55 μ m.

• In fiber optics the attenuation is commonly expressed in decibels per kilometer (dB/km). If $(Pwr)_{in}$ and $(Pwr)_{out}$ are the input and output powers, the attenuation in *decibels* is defined by

$$A = 10\log_{10} \frac{(Pwr)_{in}}{(Pwr)_{out}}$$
(9.2.30)

A 3-dB attenuation means that the output power is half the input power. In terms of an attenuation coefficient a_0 per unit length, $(Pwr)_{in}/(Pwr)_{out} = e^{a_0L}$, where L is the length of the fiber. a_0 and A are related by $A(dB) = 10 \log_{10} e^{a_0L}$, or

$$e^{a_0L} = (10^{0.434})^{a_0L} = 10^{A(dB)/10}$$
(9.2.31)

and therefore $a_0 = (0.23/L)A$ (dB) and

$$a_0(cm^{-1}) = 2.3 \times 10^{-6} A(dB/km)$$
 (9.2.32)

Decibel units are sometimes convenient simply because of the fact that the logarithm of a product of two numbers is equal to the sum of the two logarithms. For example, when a fiber with an attenuation (gain) of 10 dB is followed by a fiber with an attenuation (gain) of 20 dB, the overall attenuation (gain) is 30 dB.

The remarkable transmission capabilities of glass telecom fibers can be appreciated by a comparison with ordinary window glass, which has an optical attenuation coefficient $a_0 \sim 0.05 \text{ cm}^{-1}$, about 100,000 times that of a fiber with A = 0.2 dB/km. The small attenuation of transatlantic fiber cable allows repeaters (amplifiers) to be placed $\sim 70 \text{ km}$ apart.

The bending flexibility of fibers compared to the brittleness of bulk glass is mainly a consequence of their small surface areas. Fracture in glass and many other materials arises from voids that act to concentrate the effect of an applied stress. In glass, the voids are associated with tiny surface cracks that can grow under an applied stress and lead to fracture. The theory suggesting that the brittleness of glass is a surface effect, and therefore should be reduced when the surface area is decreased, was developed in the early 1920s by A. A. Griffith, who showed that "hot-drawing" glass into fibers dramatically increased its strength.

Fibers for guiding light had been proposed and tested in the 1920s and 1930s, but the fibers at the time were unclad and inefficient transmitters of light. The development of *fiber bundles* for "fiberscopes," the precursors of modern endoscopes, spurred renewed interest in optical fibers in the 1950s; these are also of interest for generating high powers (albeit with generally poor beam quality) by combining the outputs of single-fiber lasers. Their invention was spurred by the need in many applications to guide light around obstacles without the usual methods based on lenses and mirrors. In the first publication on fiber bundles [Nature 173, 39 (1954)], and on the use of a lower-index sheath around a single fiber, A. C. S. van Heel wrote that:

Consideration of the construction of the eye of some insects suggested another approach. If a bundle or sheaf of thin transparent fibers is cut off perpendicularly at both ends and an optical image is formed on one end, it will be seen at the other end, as the light entering one fibre can only leave this at the other end, provided leakage of light from one fibre to another of the bundle is prevented. Moreover, the cylindrical wall of each fibre must reflect the light as nearly completely as possible, because of the numerous reflexions occurring when the fibers are thin compared to their length. Preliminarly experiments ... have shown that coating the fibers with silver or any other metal yields an unsatisfactory transmission. A much better result was obtained when the fibers were coated with a layer of lower refractive index, which ensured total reflexion. This coating was isolated from the neighboring fibers by a thin coat of black paint. In this way, flexible image rods have been obtained with satisfactory transmission, a very good contrast in the end image, and with the possibility of using forms bent in any direction (up to at least 360°).

Light can escape a bent fiber: Rays incident on the corecladding interface with an angle of incidence greater than the critical angle for total internal reflection can have an angle of incidence smaller than the critical angle when they encounter a bend. Bending loss in a fiber is characterized by an attenuation coefficient α_B such that after a propagation distance l the light inside the fiber diminishes in power by the factor $e^{-\alpha_B l}$; the fraction $1 - e^{-\alpha_B l}$ of the power at l = 0 is radiated out of the fiber. Approximate calculations yield the result that α_B for a fiber mode depends on the radius of curvature R of a bend primarily through an exponential factor $e^{-2\gamma^3 R/3\beta^2} \equiv e^{-R/R_c}$, where β is the propagation constant for the mode and g is defined by (9.2.16). Bending radii much smaller than R_c will result in significant loss of power in the fiber due to radiation from the fiber. Small values of Rc make the fiber less susceptible to bending loss; R_c is a function of the core and cladding radii and refractive indices that is not in general amenable to a simple analytical form. It increases with decreasing numerical aperture and with mode order, that is, higher-order modes have greater loss for a given bending radius than the lowest-order mode. Experiments generally support the predictions of the theory, although data analyses must also account for losses associated with the tensile strength and other characteristics of a particular fiber. Rough rules of thumb are that bending radii greater than about 10 times the fiber diameter result in acceptably small radiation loss and that fibers with numerical apertures smaller than 0.06 are too sensitive to bending to be practical. In addition to "macrobending" loss, there can also be significant "microbending" loss due to small, random bending radii along the fiber.

We have already mentioned intermodal dispersion, which can cause different pulses in a fiber to overlap and thereby limit the rate at which information in the form of "0" and "1" pulses can be transmitted. While single-mode fibers do not suffer from intermodal dispersion, there are

nevertheless other types of dispersion that can limit their information transmission rate. One of these, of course, is group velocity dispersion. Another is *polarization-mode dispersion* arising from the fact that two orthogonal polarization components can have different group velocities as a consequence of the random birefringence effect described above.

9.3 Fiber amplifier and Amplifier Spontaneous emission Noise (ASE)⁶

In this section we will derive the effect of spontaneous emission noise on a laser amplifier in which the gain medium, with no mirrors, is used to amplify a weak input field. The basic engineering problem is to find the degradation of the signal-to-noise power that is caused by the (inevitable) addition of some spontaneous emission (noise) power to the amplified signal. A typical experimental situation is shown in Figure 9.17.

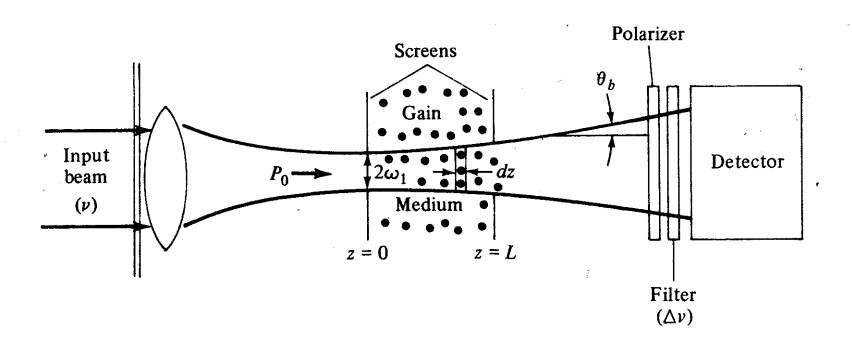


Figure 9.17: A laser amplifier consisting of an inverted atomic medium contained between two screens. The signal beam is injected so that its waist coincides with the front screen.

An inverted atomic medium with population densities N_2 and N_1 in the upper and lower transition levels occupies the space between z = 0 and z = L. An optical beam with power P is focused through an aperture with an area A_1 into the gain medium and exits through an aperture A_2 . The coherent amplification of the input beam power P due to stimulated emission is given by

$$dP = \gamma P dz \tag{9.3.1}$$

where γ , the exponential gain constant, is:

$$\gamma(\nu) = (N_2 - N_1) \frac{c^2 g(\nu)}{8\pi n^2 \nu^2 t_{\text{spont}}}$$
(9.3.2)

Let us consider next the details of how spontaneous radiation (noise) is emitted, amplified, and mixes with the signal beam to degrade its signal-to-noise ratio.

An element dz at z with area A emits spontaneously

$$P_N = \frac{N_2 h \nu A dz}{t_{\text{spont}}} \tag{9.3.3}$$

watts of power. Since this power is emitted isotropically over the 4π solid angle, only a fraction $d\Omega/4\pi$ of the total is fed into the solid angle $d\Omega$ subtended by the laser beam and ultimately intercepted by the detector. Similarly, it follows from the definition in Section 5.1 of the line-shape function $g(\nu)$ that only a fraction $g(\nu)\Delta\nu$ of the total spectrum of the spontaneous radiation falls within the transmission bandpass $\Delta\nu$ of the filter. The total noise power emitted by the elemental volume A dz within the optical spectral region $\Delta\nu$ and solid angle $d\Omega$ allowed into the detector is thus

$$(dP)' = \frac{1}{2} \frac{N_2 h \nu g(\nu) \Delta \nu A}{t_{\text{spont}}} \frac{d\Omega}{4\pi} dz$$
(9.3.4)

 $^{^6\}mathrm{Appendix}$ C (Page 730 - 732) - Optical Electronics in Modern Communications- Fifth Edition - Amnon Yariv - Oxford University Press, 1997

where the factor $\frac{1}{2}$ in front accounts for the polarizer that can remove half of the (isotropically polarized) noise without affecting the (linearly polarized) signal power. The smallest solid angle $d\Omega$ that we can use without sacrificing signal power is that subtended by the beam

$$(d\Omega)_{min} = (d\Omega)_b = \pi \theta_b^2 = \frac{\lambda^2}{n^2 A}$$
(9.3.5)

where $A = \pi \omega_1^2$ and $\theta_b = \lambda/\pi \omega_1 n$ is the far-field diffraction angle of the signal beam as shown in Figure 9.17. The value $\lambda^2/n^2 A$ is often referred to as the *solid angle per mode*.

Using (9.3.1) and (9.3.5), we rewrite (9.3.4) as

$$(dP)' = \frac{1}{2} \frac{N_2 \gamma h \nu}{N_2 - N_1} \tag{9.3.6}$$

The total evolution of beam power including the induced and spontaneous transitions is thus given by the sum of the emitted powers. (If the two contributions were coherent we would add their fields.)

$$\boxed{\frac{dP}{dz} = \gamma P + \frac{N_2}{N_2 - N_1} \gamma h \nu \Delta \nu}$$
(9.3.7)

The solution of (9.3.7) subject to the boundary condition $P(0) = P_0$ is

$$P(z) = \underbrace{P_0 e^{\gamma z}}_{\text{amplified signal}} + \underbrace{\mu h \nu \Delta \nu (e^{\gamma z} - 1)}_{\text{amplified noise}}$$
(9.3.8)

where

$$\mu \equiv \frac{N_2}{N_2 - N_1} \tag{9.3.9}$$

is the population inversion factor. The signal-to-noise power ratio at the output of the amplifier is

$$\left[\left(\frac{S}{N} \right)_{\text{output}} = \frac{P_0}{\mu h \nu \Delta \nu} \frac{G}{G - 1} \right] \tag{9.3.10}$$

 $G \equiv e^{\gamma L}$ is the one-pass gain. From the point of view of power bookkeeping, the effect of spontaneous emission is seen to be equivalent to a noise input power

$$N_{\text{eff}} = \mu h \nu d\nu \left(1 - \frac{1}{G}\right) \tag{9.3.11}$$

which for an ideal four-level gain medium $(\mu = 1)$ and high gain $(G \gg 1)$ becomes

$$N_{\text{eff}}h\nu\Delta\nu$$
 (9.3.12)

If the laser amplifier were to be employed as a preamplifier in an optical receiver, then the minimum detectable power is given by

$$(P_s)_{min} \sim h\nu\Delta\nu \tag{9.3.13}$$

9.4 Noise figure of an Fiber Amplifier ⁷

The degradation of the SNR after passage through an optical amplifier is quantified in terms of the noise figure, F, defined as

$$F = \frac{\text{SNR}_{in}}{\text{SNR}_{out}}$$
(9.4.1)

In the discussions that follow, the noise figure in decibels is determined according to: $F = 10 \log(F)$. The SNRs are referred to the output of an ideal photodetector which is capable of converting each photon of incident light into electrical current (in other words, 100% quantum efficiency). The

 $^{^{7}\}mathrm{Chapter}$ 13 (Page 542 - 546) - Fiber optic test and measurement - Derickson, Dennis- New Jersey : Prentice Hall, 1998

input SNR is defined to be that from a shot-noise-limited source. The shot-noise-limited input reference is critical to the definition. If an optical source with a large amount of intensity noise were used to measure the noise figure of an amplifier. the amplified source noise would dominate over the amplifiers own noise contribution and lead to an erroneous noise figure of 0 dB, in other words, no observed SNR degradation caused by the amplifier.

The noise figure concept is illustrated in Figure 9.18. The input SNR is determined with the amplifier bypassed using an idealized source and receiver. The amplifier is inserted and the output SNR is determined. Equation (9.4.1) is next used to calculate the amplifier noise figure. The idealized source is shot-noise-limited and set to the appropriate power, wavelength, and Iinewidth. The

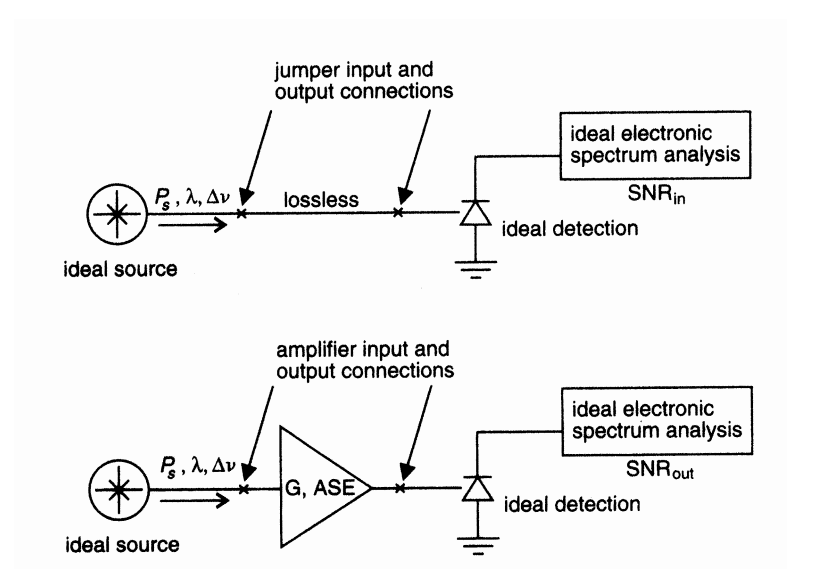


Figure 9.18: Noise figure concept in terms of idealized source and receiver.

idealized receiver has a calibrated frequency response and contributes no excess noise of its own. Obviously the real world is not yet ideal and much of the work involving noise figure measurements is in dealing with the source and the receiver non-idealities.

The 3 dB Noise-Figure Myth

A minimum 3 dB (actually, $\log_{10}(2) = 3.01$ dB) amplifier noise figure is sometimes attributed to the EDF A. If taken out of context this can result in a considerable misunderstanding of the EDFA noise performance. To better understand where the 3 dB limit originates, let us examine the noise figure under moderate signal conditions as the amplifier gain varies. Moderate signal conditions imply that the signal power is much greater than the ASE power in the optical bandwidth of interest. This ensures that the sig-sp beat noise dominates over that of the sp-sp beat noise as indicated by Figure 13.17. Consider the case of a fiber amplifier where initially there are no erbium ions in the "active" optical fiber. Discounting any loss in the optical fiber, the noise figure is unity, in other words, no SNR degradation since the signal passes from amplifier input to output unchanged. As the erbium-ion-doping increases, so does the optical gain, the ASE level, and the signal level. The noise figure increases from 0 dB to 3 dB, or beyond, if other noise sources or optical losses are present. This can be seen from the equation for sig-sp beat noise and shot-noise-limited noise figure derived by

$$F = 2n_{sp}\frac{(G-1)}{G} + \frac{1}{G}$$
(9.4.2)

which for large gains yields: $F \approx 2n_{sp}$ where the SE factor, $n_{sp} \leq 1$. A fully inverted amplifier can be achieved with 980 nm pumping resulting in an effective SE factor of unity which leads to a noise figure of 3 dB. Equation (9.4.2) is plotted versus gain in Figure 9.19. From the figure, a fully inverted amplifier (in other words, $n_{sp} = 1$) with 4 dB of gain and zero input coupling loss has a noise figure near 2 dB. The 3 dB value is the limit for a high-gain amplifier with zero input coupling

loss and a fully inverted amplifying fiber. Any loss near the amplifier input, or departure from complete inversion will cause the noise figure to exceed 3 dB. gain amplifiers such as the EDFA.

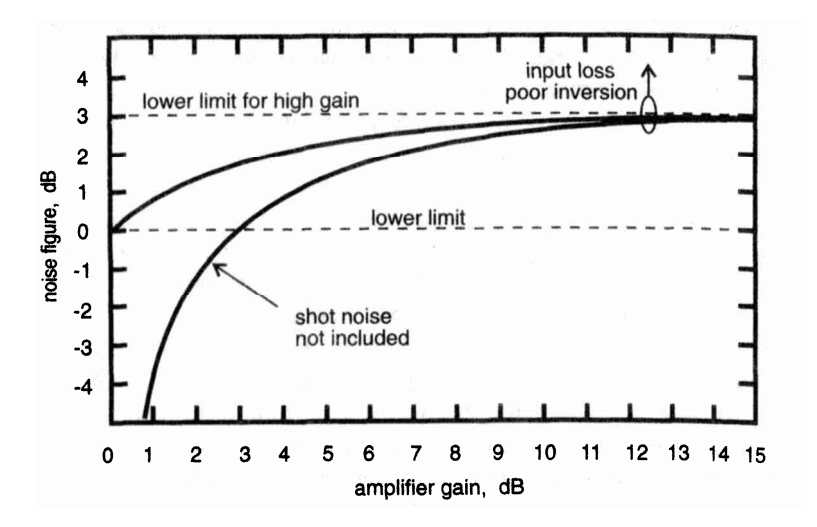


Figure 9.19: Noise figure dependence on optical amplifier gain with and without the shot-noise contribution.

In calculations with concatenations of amplifiers, it is convenient to suppress the shot noise until the signals are analyzed at the detector. In the calculation of noise, figure for a single amplifier, failure to include the shot noise will result in significant error in the gain regime below 15 dB.